GDCh

**Research Articles**

*Angewandte*
*Chemie*
International Edition
www.angewandte.org

Check for updates

**Zn-Ion Batteries**

# When It's Heavier: Interfacial and Solvation Chemistry of Isotopes in Aqueous Electrolytes for Zn-ion Batteries

*Xuan Gao+, Yuhang Dai+, Chengyi Zhang, Yixuan Zhang, Wei Zong, Wei Zhang,
Ruwei Chen, Jiexin Zhu, Xueying Hu, Mingyue Wang, Ruizhe Chen, Zijuan Du, Fei Guo,
Haobo Dong, Yiyang Liu, Hongzhen He, Siyu Zhao, Fangjia Zhao, Jianwei Li,
Ivan P. Parkin, Claire J. Carmalt, and Guanjie He\**

**Abstract:** The electrochemical effect of isotope (EEI) of water is introduced in the Zn-ion batteries (ZIBs) electrolyte to deal with the challenge of severe side reactions and massive gas production. Due to the low diffusion and strong coordination of ions in $D_2O$, the possibility of side reactions is decreased, resulting in a broader electrochemically stable potential window, less pH change, and less zinc hydroxide sulfate (ZHS) generation during cycling. Moreover, we demonstrate that $D_2O$ eliminates the different ZHS phases generated by the change of bound water during cycling because of the consistently low local ion and molecule concentration, resulting in a stable interface between the electrode and electrolyte. The full cells with $D_2O$-based electrolyte demonstrated more stable cycling performance which displayed ~100% reversible efficiencies after 1,000 cycles with a wide voltage window of 0.8–2.0 V and 3,000 cycles with a normal voltage window of 0.8–1.9 V at a current density of $2\,A\,g^{-1}$.

## Introduction

Aqueous electrolytes have been viewed as promising components for electrochemical energy storage application due to their low cost, ease of usage, and safety. With the advantages of excellent industrial adaptability and high energy density, aqueous Zn-ion batteries (ZIBs) have been increasingly studied among the aqueous energy storage technologies in recent years.[1] When the water is utilized as the electrolyte in ZIBs, it confers a high ionic conductivity because of large acceptor number (AN, 54.8) and donor number (DN, 18) as well as the high dielectric constant (78 at 25°C).[2] However, the practical application of aqueous electrolytes is restricted by their narrow electrochemically stable potential window of 1.23 V for pure water, due to the hydrogen evolution reaction (HER) and the oxygen evolution reaction (OER).[3] To provide a wide operating voltage range for aqueous ZIBs, neutral salts, particularly sulphates with significant hydration with water molecules to create an energy barrier for water electrolysis, have been produced.[4] On the basis of this salt-dependent hydration mechanism, recent research in aqueous electrolytes has increased the electrochemical window (EW) by modifying the solvation structure, property, and concentration of the salt component of aqueous electrolytes.[5] On the other hand, the complex side reactions in ZIBs seriously interfere with the stable cycle, which has become a great challenge for aqueous energy storage technology.[6] Researchers have made lots of efforts developing various organic and inorganic electrolyte additives to alleviate the side reactions, so as to alleviate the gas production, pH changes and the generation of side productions, such as zinc hydroxide sulfate hydrate (ZHS) during the cycle.[7] From the perspective of industrialization, the high-cost production lines also require the introduction of additives that are easy to store and have limited influence on the battery charge and discharge behavior.

Apart from the electrolyte additive, the application of isotope effect in electrochemical energy storage technology is another promising direction to increase the potential window and cycling stability. Prof. Frederick Soddy used the term "isotope" in 1913 to describe two or more atoms that

[*] X. Gao,+ W. Zong, W. Zhang, X. Hu, M. Wang, R. Chen, Z. Du,
F. Zhao, I. P. Parkin, C. J. Carmalt, G. He
Christopher Ingold Laboratory, Department of Chemistry, University
College London
20 Gordon Street, London, WC1H 0AJ (UK)
E-mail: g.he@ucl.ac.uk

X. Gao,+ Y. Dai,+ R. Chen, J. Zhu, F. Guo, H. Dong, Y. Liu, H. He,
S. Zhao, J. Li
Department of Chemical Engineering, University College London
London WC1E 7JE (UK)

C. Zhang
Institute of Technological Sciences, Wuhan University
Hubei, Wuhan, 430072 (P. R. China)

Y. Zhang
Institute of Materials Science, Technische Universität Darmstadt
64287 Darmstadt (Germany)

[+] These authors contributed equally to this work.

share the same atomic number (number of protons/electrons) but have distinct nucleon numbers (mass numbers) because they have different numbers of neutrons in their nucleus.[8] These isotopes have the same chemical element but distinct atomic masses. The nuclear charge and electron configuration of an atom are determined by the number of protons, and the stable (non-radioactive) isotopes of an element and their compounds typically exhibit comparable physicochemical characteristics.[9] However, the isotope effect, which is caused by different mass and nuclear spin of the isotopes, can affect the thermodynamic and kinetic parameters of a chemical reaction, such as the equilibrium constant, and can result in differences in the physical properties of an element or compound (such as density, vapor pressure, and melting point).[10] As there is a significantly greater mass difference between the isotopes for the light elements, the isotope effects are more pronounced. The two stable natural isotopes of hydrogen, protium ($^1H$) and deuterium ($^2H$ or D), are the lightest elements in the Periodic Table.[11] Protium and deuterium both have one proton, but deuterium contains an extra neutron in its nucleus, increasing its atomic mass by roughly 100 %. The hydrogen element and its derivatives exhibit strong isotope effects, which are explained by the enormous difference in atomic mass. Deuterium oxide ($D_2O$, often known as heavy water) exhibits noticeably different physicochemical features when compared to protium oxide ($H_2O$, or water), as seen in Table S1. From the perspective of $D_2O$ molecular, the isotopic effect is greatly influenced by intermolecular hydrogen bonding. The hydrogen bonds between $H_2O$ molecules are longer and less angular than those between $D_2O$ molecules due to the significant larger quality of D and the D-bond energy of $D_2O$ is 1 $kJ\,mol^{-1}$ larger than H-bond energy of $H_2O$ based on the previous studies.[3] With two lone pairs of electrons and two hydrogen atoms, a water molecule can interact with four surrounding water molecules to form a tetrahedral hydrogen-bond network. Compared with $H_2O$, the tetrahedron formed by $D_2O$ is more symmetrical, which is favorable for the formation of D-bonds. Additionally, $D_2O$ shows a higher dissociation energy ($E_d$) than $H_2O$ because the two molecules have the same total potential energy.[3,12]

In this study, the electrochemical effect of isotope (EEI) is applied to the electrolyte of ZIBs for the first time to alleviate the side reaction and enhance the stability during the cycle. From a kinetic study perspective, molecular dynamics (MD) simulations of EEI in $D_2O$ and $H_2O$ were first performed and the low diffusion coefficient of ions in $D_2O$ was discovered to demonstrate the promising potential of $D_2O$-based electrolytes in ZIBs. Due to the low diffusion coefficient and strong coordination of ions in $D_2O$, the probability of side reactions in the battery is reduced, exhibiting a wider EW, less pH variation, and less ZHS generation during cycling. More notably, the $D_2O$ environment can mediate the phase of ZHS during cycling. Here, we found for the first time that $D_2O$ suppresses the generation of different phases of ZHS induced by the change of bound water in ZHS during cycling, providing a more stable electrode-electrolyte interface. The full cells

with $D_2O$-based electrolytes exhibited more stable cycling performance than $H_2O$-based electrolytes, and exhibited ~100 % reversible efficiencies after 1,000 cycles with a voltage window of 0.8–2.0 V and 3,000 cycles with a normal voltage window of 0.8–1.9 V.

## Results and Discussion

As shown in Figure 1a, the $D_2O$-based electrolyte alleviates the side reactions of ZIBs during cycling and can be attributed to three aspects: low diffusion of molecules/ions, strong coordination between ions and $D_2O$, and strong O–D bonds. From the perspective of the anode, the low diffusion of $Zn^{2+}$ in $D_2O$ slows down the formation of Zn dendrites, making the interface formed by $Zn^{2+}$ deposition flat. At the cathode, the EEI of $D_2O$ regulates the interface between the cathode and the electrolyte by controlling the bound water in the ZHS structure and the amount of ZHS. First-principles calculations were performed to reveal the underlying mechanism when different solutes were adopted. As the growth of Zn dendrites and LDH is often closely related to the OER and HER on the anode surface, we first investigated the thermodynamic behavior on the metallic Zn anode surface. As evidenced by Figures S1a and b, it is clear that the adsorption of H, D, or OH, OD on the surface of Zn remains essentially the same. As the adsorption of H or OH on the electrode surface is the key step in the HER and OER, respectively, the adsorption energy and differential charge density difference diagrams provide sufficient evidence that there is no significant difference in the thermodynamic response of the two different electrolytes on the surface of the electrodes. We also performed the MD for the investigation of the bulk phase of the electrolyte in Figure S1c. However, no difference in the radial distribution function was indicated. The results fully demonstrate that despite the change in the electrolyte, there is no change in the thermodynamic behavior of the system.

Further, the behavior differences between $D_2O$ and $H_2O$ in ZIBs were investigated from a kinetic point of view. We make the long-enough MD simulation to understand bulk electrolytes and their influence on the surface of the anode. As presented in Figure 1c, the diffusion coefficient of $Zn^{2+}$ in the $D_2O$ and $H_2O$ are 0.22 and 0.32, respectively, which indicates the drop in the ionic conductivity. Furthermore, the diffusion coefficient of $D_2O$ (0.1171) in solution is significantly lower than that of $H_2O$ (0.3238), indicating that the $D_2O$ solution, despite the reduction in ionic conductivity, slows down the mass transfer of electrolyte at the electrode surface, effectively inhibiting the side reactions and the formation of $H_2$. Moreover, the kinetic diffusion behaviors of the electrolytes for HER (H, D) and OER (OH, OD) were studied. The lower diffusion coefficients of the D ($3.724\times10^2$) and OD ($3.202\times10^4$) make it difficult to couple with another D or OD for the further step in the HER or OER compared to the H ($5.688\times10^2$) and OH ($3.984\times10^4$). Both sluggish kinetic behavior of the D, OD, and $D_2O$ in the bulk phase of the electrolyte and the surface on the anode greatly restrain the side-reaction in the aqueous battery
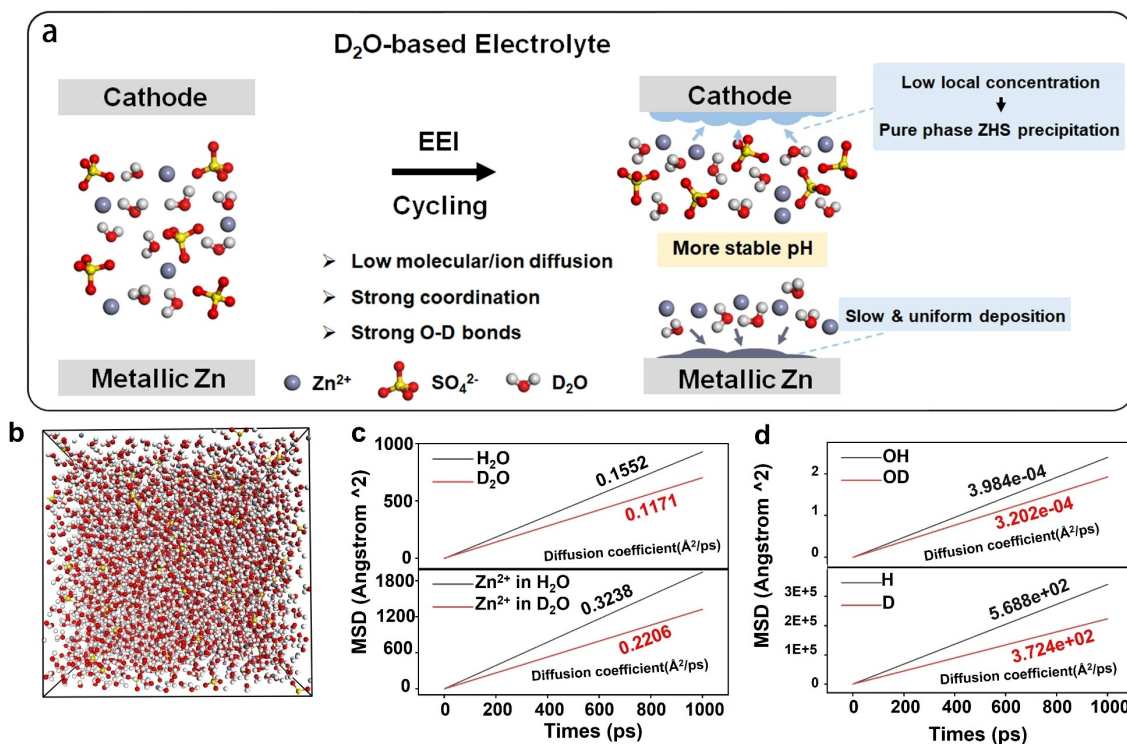
**Figure 1.** (a) Schematic diagram illustrating the influence from EEI of $D_2O$. (b) The configuration of the electrolyte. (c) The mean square displacements (MSD) of $Zn^{2+}$, $H_2O$, and $D_2O$ in the corresponding electrolyte. (d) The MSD of the OH, OD, H and D on the surface of the metallic Zn.

systems. In addition to the traditional trail-and-error approach for the optimization of the thermodynamic behavior of materials. Our investigation has proposed the new idea that improving the behavior of the reaction kinetics is also a long-lasting and effective route.

The isotopic effect of hydrogen also affects the electrochemical properties of water.[13] The commonly used electrolyte for ZIBs, 2 M zinc sulfate heptahydrate ($ZnSO_4 \cdot 7H_2O$) was prepared in $H_2O$ and $D_2O$, respectively. By observing and comparing the Fourier-transform infrared spectroscopy (FTIR) in Figure 2a, it can be found that the $D_2O$ and $H_2O$ hydroxide ion peak positions in the electrolyte are greatly different. The FTIR spectra of $ZnSO_4$ in $H_2O$ showed the presence of the absorption bands at 3115 and 1612 $cm^{-1}$ for stretching and bending vibrations of $H_2O$ molecules, respectively.[14] Correspondingly, the stretching and bending vibrations of $D_2O$ molecules are at 2468, 1442 and 1205 $cm^{-1}$, respectively.[15] The bands observed at 1091 $cm^{-1}$ in $H_2O$, 1201 and 1091 $cm^{-1}$ at $D_2O$ indicate the asymmetric stretching mode of $SO_4^{2-}{}_{v3}$.[15] The absorption presented at 605 $cm^{-1}$ indicates asymmetric bending mode of $SO_4^{2-}{}_{v4}$.[16] The small amount of stretching and bending vibrations of $H_2O$ in the $D_2O$-based electrolyte corresponds to the crystal water introduced during the preparation of the solution. As a common additive, manganese sulfate ($MnSO_4$) was investigated whether it influences the absorption within the electrolyte, as shown in Figure S2a. The introduction of $Mn^{2+}$ has little effect on the absorption behavior in the electrolyte and shows no peak shift. To investigate the

electrochemical behavior of $D_2O$-based electrolyte, Zn||Ti cells were assembled to compare the EW of $H_2O$ and $D_2O$ during the $Zn^{2+}$ deposition process. At room temperature, the ionic conductivity of $D_2O$-based electrolytes is slightly lower than that of $H_2O$-based electrolytes, which has been demonstrated in previous studies.[3,12,17] Simultaneously, the strong coordination between $D_2O$ and $Zn^{2+}$ increases the proportion of coordinated water. The increase in the number of neutrons in deuterium atoms in $D_2O$ can significantly expand the EW of aqueous electrolytes because of the lower zero-point energy of deuterium compounds, smaller ionic products, and larger dehydration energy of $D_2O$.[12] As shown in Figure 2b, 2 M $ZnSO_4 \cdot 7H_2O$ was dissolved in $H_2O$ and $D_2O$, respectively, to explore the difference in aqueous electrolyte caused by EEI. Verified by linear sweep voltammetry (LSV) tests at a sweep rate of 10 $mV\,s^{-1}$, $D_2O$ was able to significantly inhibit OER. As shown in Figure 2c, the potential gap of Zn deposition between $D_2O$ and $H_2O$ is only 0.02 V, indicating that it has no significant effect on the deposition potential of $Zn^{2+}$ on metallic Zn. However, the potential of HER is significantly different between $D_2O$- and $H_2O$-based electrolyte. The potential of HER in $D_2O$ is 0.1 V lower than that of $H_2O$, indicating that $D_2O$ can inhibit HER. Based on the EEI, we found that the potential window of the $ZnSO_4$ aqueous electrolyte is extended by $\sim 9.98\%$, which can be attributed to the increase in the number of neutrons in deuterium atoms relative to protium. To further explore the effect of EEI on $Zn^{2+}$ deposition, The Zn–Zn symmetry cell was
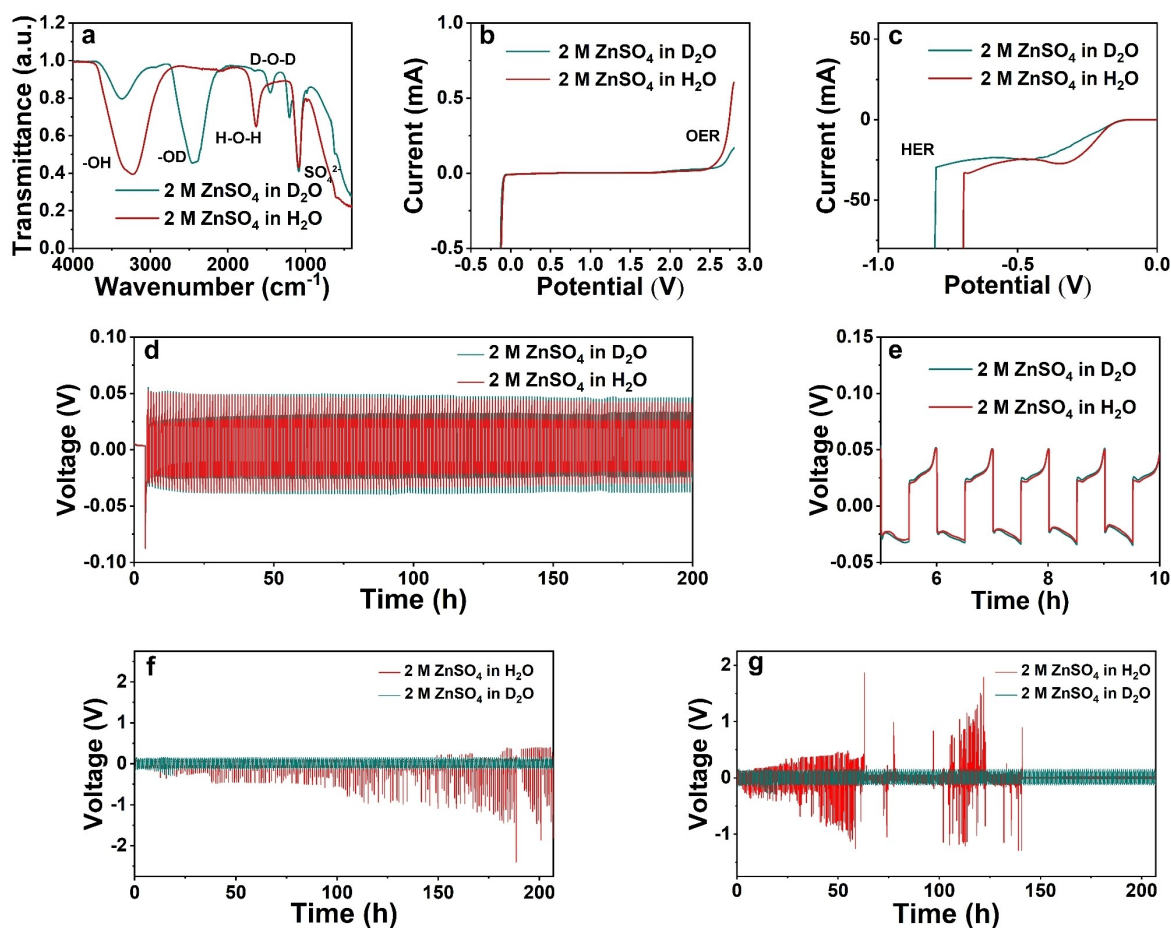
***Figure 2.*** (a) FTIR spectra of 2 M ZnSO$_4$ in D$_2$O and H$_2$O, respectively. (b) LSV test of 2 M ZnSO$_4$ in D$_2$O and H$_2$O in Zn‖Ti cells and (c) a focus on Zn deposition. Cycling performance of Zn‖Zn symmetric cells at (d) 5 mA cm$^{-2}$ for 1 mAh cm$^{-2}$ with (e) an enlarged period of the 5$^{th}$-10$^{th}$ h, (f) 20 mA cm$^{-2}$ for 10 mAh cm$^{-2}$ and (g) 40 mA cm$^{-2}$ for 10 mAh cm$^{-2}$.

tested by cyclic voltammetry (CV) in Figure S2b. The D$_2$O-based electrolyte exhibits a slower deposition process than the H$_2$O-based electrolyte. To analyze the cause of EEI in water solvent, on one hand, according to the principle of energy conservation, the overall energy change in the electrode reaction can be simply expressed as the Born-Haber cycle.[18] Since the activation energy of D$_2$O is higher than that of H$_2$O, the electrolysis of water in D$_2$O is inhibited when factors such as the electron work function and hydration energy of the electrodes are considered. On the other hand, due to the non-negligible effect of kinetics, the low diffusion coefficient of ions in the electrolyte results in a low reaction rate and reduces the reactivity at the electrolyte-electrode interface.

As shown in Figure 2d, the D$_2$O-based and H$_2$O-based electrolytes behave similarly in the initial polarization part of the Zn‖Zn symmetric cells at a current density of 5 mA cm$^{-2}$ for 1 mAh cm$^{-2}$, while the overpotential of the D$_2$O-based electrolyte is slightly higher than that of the H$_2$O-based electrolyte. With the increase of cycle time, from 50 h, the ZIBs with H$_2$O-based electrolyte begins to show a significant decrease in overpotential, which can be attributed to the growth of dendrites generated by the irreversible

deposition of Zn$^{2+}$ between the electrodes, resulting in a reduced overpotential.[19] The D$_2$O-based electrolyte can maintain a stable overpotential value throughout the 200-h cycle, indicating that the phenomenon of the effect of the distance between the electrodes caused by the irreversible deposition of Zn$^{2+}$ has slowed down.[20] To a certain extent, it also shows that the Zn$^{2+}$ in H$_2$O are more prone to aggregate deposition than Zn$^{2+}$ in D$_2$O. Based on the kinetic studies, due to the lower diffusion coefficient of Zn$^{2+}$ in D$_2$O, Zn$^{2+}$ will choose a closer location to deposit rather than deposit at the tip to form a dendrite. In addition, the overpotential of the Zn‖Zn symmetric cells with H$_2$O-based electrolyte exacerbates the asymmetry during cycling, which indicates that a considerable amount of irreversible deposition has occurred at the metallic Zn electrode on one side.[21] As shown in Figure 2e, ZIBs with D$_2$O-based electrolyte exhibits a higher initial Zn deposition barrier, which can be attributed to the lower ionic conductivity of D$_2$O and the relatively low diffusivity of Zn$^{2+}$ in D$_2$O.[22] Such a difference in kinetics also leads to a slightly higher overpotential in the initial stage of the ZIBs with D$_2$O-based electrolyte than the one with H$_2$O-based electrolyte. After 50 h of cycling, the metallic Zn electrodes were taken out to

compare the surface morphology, and the presence of flower-like dendrites was still observed in Zn||Zn symmetric cell with the $D_2O$-based electrolyte, as shown in Figures S3a and b. In the Zn||Zn symmetric cell with $H_2O$-based electrolyte, a large amount of uneven ZHS covered the electrode surface, as shown in Figure S3c. However, the electrodes cycled in $D_2O$-based electrolyte showed smooth surface morphology. To examine the cycling stability of the $D_2O$-based electrolyte at high current densities, Zn||Zn symmetric cells were tested at the conditions of $20\,mA\,cm^{-2}$ for $10\,mAh\,cm^{-2}$ and $40\,mA\,cm^{-2}$ for $10\,mAh\,cm^{-2}$, as shown in Figure 2f and g. The $H_2O$-based electrolyte is difficult to cycle at such high current densities, while the $D_2O$-based electrolyte is even able to cycle for more than $200\,h$ under the harsh condition of $40\,mA\,cm^{-2}$ for $10\,mAh\,cm^{-2}$. A 1:1 mixture of $D_2O$ and $H_2O$ was prepared as an electrolyte for further study on the Zn||Zn symmetric cell at $10\,mA\,cm^{-2}$ for $1\,mAh\,cm^{-2}$, as shown in Figure S4. Since D and H belong to isotopes, $D_2O$ and $H_2O$ can be infinitely miscible, which provides the possibility of flexible mixture ratio. From Figure S4, it can be clearly found that the mixing of $D_2O$ and $H_2O$ shows a more durable cycling performance and a slower overpotential reduction trend than $H_2O$. Meanwhile, the electrochemical stable potential window of the electro-lyte prepared by the mixture is slightly smaller than that of the pure $D_2O$-based electrolyte.

Figure 3a shows the in situ optical microscopy of electroplating process of Zn at a current density of $1\,mA\,cm^{-2}$ with $2\,M$ $ZnSO_4$ in $D_2O$ as the electrolyte. As a control, $2\,M$ $ZnSO_4$ was dissolved in $H_2O$ as the electrolyte for in situ optical microscopy observation under the same conditions, as shown in Figure 3b. Both for $D_2O$- and $H_2O$-based electrolytes, Zn deposits formed on the surface layer after electroplating at a current density of $1\,mA\,cm^{-2}$ for $30\,min$. The Zn deposition thickens significantly with increasing plating time. From the case of $10\,min$, thicker Zn deposition has been exhibited in the $H_2O$-based electrolyte, and $Zn^{2+}$ are preferentially deposited on the tips of the initial protrusions. At $30\,min$, dendrites with a length of about $200\,\mu m$ have appeared in the $H_2O$-based electrolyte. It is obvious that the Zn deposition in the $D_2O$-based electrolyte is thinner and flatter than of the one in $H_2O$-based electrolyte after $30\,min$. Since the $Zn^{2+}$ is electroplated on the surface, this indicates that the $D_2O$-based electrolyte is easier to suppress the uneven Zn dendrites than the $H_2O$-based electrolyte.[23] To further explore the effect of EEI on Zn electroplating, the side-view scanning electron microscope (SEM) images of the metallic Zn electrode surface after $30\,min$ deposition in $D_2O$-based and $H_2O$-based
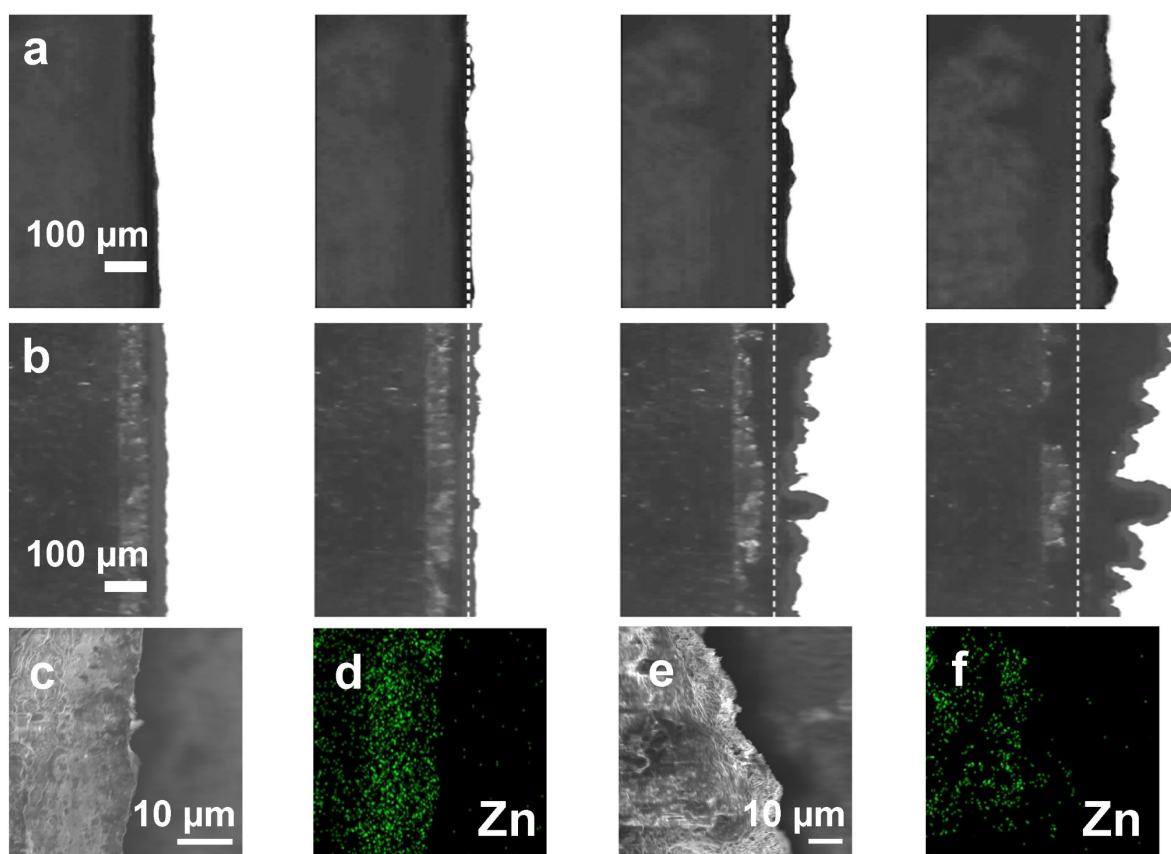


***Figure 3.*** In situ optical microscope at 0, 10, 20, 30 min of electroplating process of Zn in (a) $D_2O$-based and (b) $H_2O$-based electrolytes, indicating $D_2O$ is able to suppress the length of Zn dendrites. (c, e) Side-view SEM images and (d, f) corresponding EDS mapping of the metallic Zn electrode surface after 30 min deposition in $D_2O$-based and $H_2O$-based electrolytes.

electrolytes are shown in Figures i and k, respectively. The metallic Zn electrode surface in the D$_2$O-based electrolyte is very smooth and uniform, indicating its excellent ability to promote uniform deposition of Zn$^{2+}$. As shown in the energy dispersive spectrometry (EDS) mapping in Figure 3c, the Zn element can be uniformly distributed on the electrode surface. In sharp contrast, as shown in Figure 3e, the Zn electroplating in the H$_2$O-based electrolyte is not as smooth as that of D$_2$O-based electrolyte, with significant unevenness on its surface, resulting in a distinctly different light-dark contrast in the SEM images. In addition, the distribution of Zn element, as shown in Figure 3f, also shows the inhomogeneous deposition of Zn$^{2+}$.

The Zn||MnO$_2$ full cells were assembled to further understand the EEI effect. Previous studies have demonstrated that the pH value of aqueous batteries can significantly affect their cycling performance, especially MnO$_2$-based ZIBs. The in situ pH values of 2 M ZnSO$_4$ in D$_2$O and H$_2$O, respectively, were measured and incorporated in Figure 4a. The initial pH values of 2 M ZnSO$_4$ dissolved in D$_2$O, and H$_2$O are about 4.18 and 4.15, respectively, and the difference is not obvious. However, after 10 cycles at a constant current density of 2 A g$^{-1}$, the pH value of the D$_2$O-based electrolyte increased to 5.41, which was slightly higher than the pH value of 5.1 of the H$_2$O-based electrolytes. During the subsequent cycling, the pH value of the D$_2$O-based electrolyte was stable at 5.45, while the pH value of the H$_2$O-based electrolyte gradually increased to 6.05, which is consistent with previous studies. In ZIBs with MnO$_2$ cathodes, the process of influencing pH value can be summarized in Table S2.

The EEI on the pH value change in the electrolyte is mainly due to the inertness caused by the deuterium atom.[24] Since MnO$_2$ is used as the cathode, the charge–discharge process of ZIBs is more understood as the intercalation and extraction of protons, Zn$^{2+}$, and the deposition and dissolution of Mn$^{2+}$, which is a complicated process. When an acidic electrolyte is applied, Mn$^{IV}$O$_2$ tends to react with protons (derived from water) and gain an electron to generate, Mn$^{III}$OOH, a process corresponding to the intercalation and deintercalation of protons, as shown in Eqn. 1.[25]

$$2Mn^{III}OOH + 2H^+ \rightarrow Mn^{IV}O_2 +\ Mn^{2+} + 2H_2 \tag{1}$$
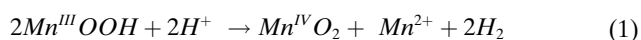
However, as shown in Eqn. 1, Mn$^{III}$OOH tends to continue to react with protons to form H$_2$. This process irreversibly consumes protons and raises the pH value.[26] When the pH value continues to rise, Zn$^{2+}$, Mn$^{2+}$ and OH$^-$ in the electrolyte tend to form ZnMn$_2$O$_4$, which is less reversible, as shown in Eqn. 2.

$$3Zn^{2+}\ 6Mn^{2+} + 24OH^- \rightleftharpoons 3ZnMn_2O_4 + 12H_2O\ + 6e^- \tag{2}$$
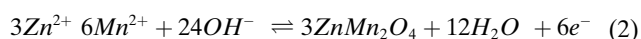
The resulting ZnMn$_2$O$_4$ hinders the contact between the cathode and the electrolyte due to its poor electrical activity, resulting in irreversible capacity loss.[27] However, because the formation of ZnMn$_2$O$_4$ hinders the contact between the active material and the protons in the electrolyte, the pH value of the electrolyte tends to be flat and reaches an equilibrium value. In H$_2$O-based electrolytes, this equilibrium pH is near 6. In the D$_2$O-based electrolyte, EEI makes the deuteron more inert, which alleviates the reaction of Mn$^{III}$OOH with D$^+$. On the other hand, due to the low diffusion coefficient of Zn$^{2+}$ and OD$^-$ in D$_2$O, the chemical reaction slows down. However, when the pH value increases, the D$_2$O-based electrolyte attenuates the positive reaction rate in Eqn. 2 due to the lower concentration of free OD$^-$ near the electrode surface, thus reaching equilibrium at a lower pH value. Therefore, from the perspective of the full cell, the D$_2$O-based electrolyte is able to well alleviate the pH value change during cycling. The reaction rate of HER and OER is reduced due to EEI, which is determined by the lower diffusion of OD$^-$, D$^+$ in the electrolyte and the higher reaction barrier simultaneously, reducing the production of H$_2$ and O$_2$.

Another major challenge of ZIBs research when MnO$_2$ acts as a cathode is the generation of ZHS during cycling, and this poorly reversible precipitation hinders the effective contact between the electrode and the electrolyte.[28] Many efforts have been made in the past to mitigate ZHS formation, and many electrolyte additives have been investigated.[29] But this may make the researchers ignore the discussion of the solvent itself. Ex situ X-ray diffraction (XRD) was used to compare the amount and structure of ZHS generated during cycling in D$_2$O-based and H$_2$O-based electrolytes. The different states in Figures 4c and e are marked in Figure 4b. When D$_2$O was used as the electrolyte solvent in the MnO$_2$-based full cell, the formation of ZHS was significantly reduced, as shown in Figures 4c and e. To eliminate the influence of active material mass loading, temperature and other factors, it is ensured that the active material loading in the cathode is $1 \pm 0.05$ mg cm$^{-2}$ and the tested full cell is simultaneously cycled at a current density of 2 A g$^{-1}$. The intensity ratio of the highest peak (001) of ZHS in D$_2$O-based to the carbon paper peak ($\sim 26°$) is 1.73. While the height ratio of the highest peak (001) of ZHS in H$_2$O-based to the same peak is 4.17. Due to the limitations of the test, the generation of ZHS cannot be fully quantified, but the generation of ZHS in the H$_2$O-based electrolyte is significantly higher than that in the D$_2$O-based electrolyte. More notably, as shown in Figure 4d, the ZHS generated in the D$_2$O-based electrolyte is Zn$_2$(OH)$_2$SO$_4 \cdot$4H$_2$O (ICDD No. 00-044-0673), which is caused by the lower amount of free water molecule in D$_2$O.[27b] For comparison, Figure 4f shows that relatively pure Zn$_2$(OH)$_2$SO$_4 \cdot$5H$_2$O (ICDD No. 00-039-0688) is generated in the H$_2$O-based electrolyte only during the first discharge. With the increase of cycle numbers, the generated ZHS mostly consists of a mixed phase composed of Zn$_2$(OH)$_2$SO$_4 \cdot$4H$_2$O and Zn$_2$-(OH)$_2$SO$_4 \cdot$5H$_2$O.[27b]

The generation of ZHS with different structures during cycling may be an easily overlooked but an important factor affecting the cycling performance of ZIBs. As shown in Figure 4g, the phase of generated ZHS can be explained by local concentration of water mole-
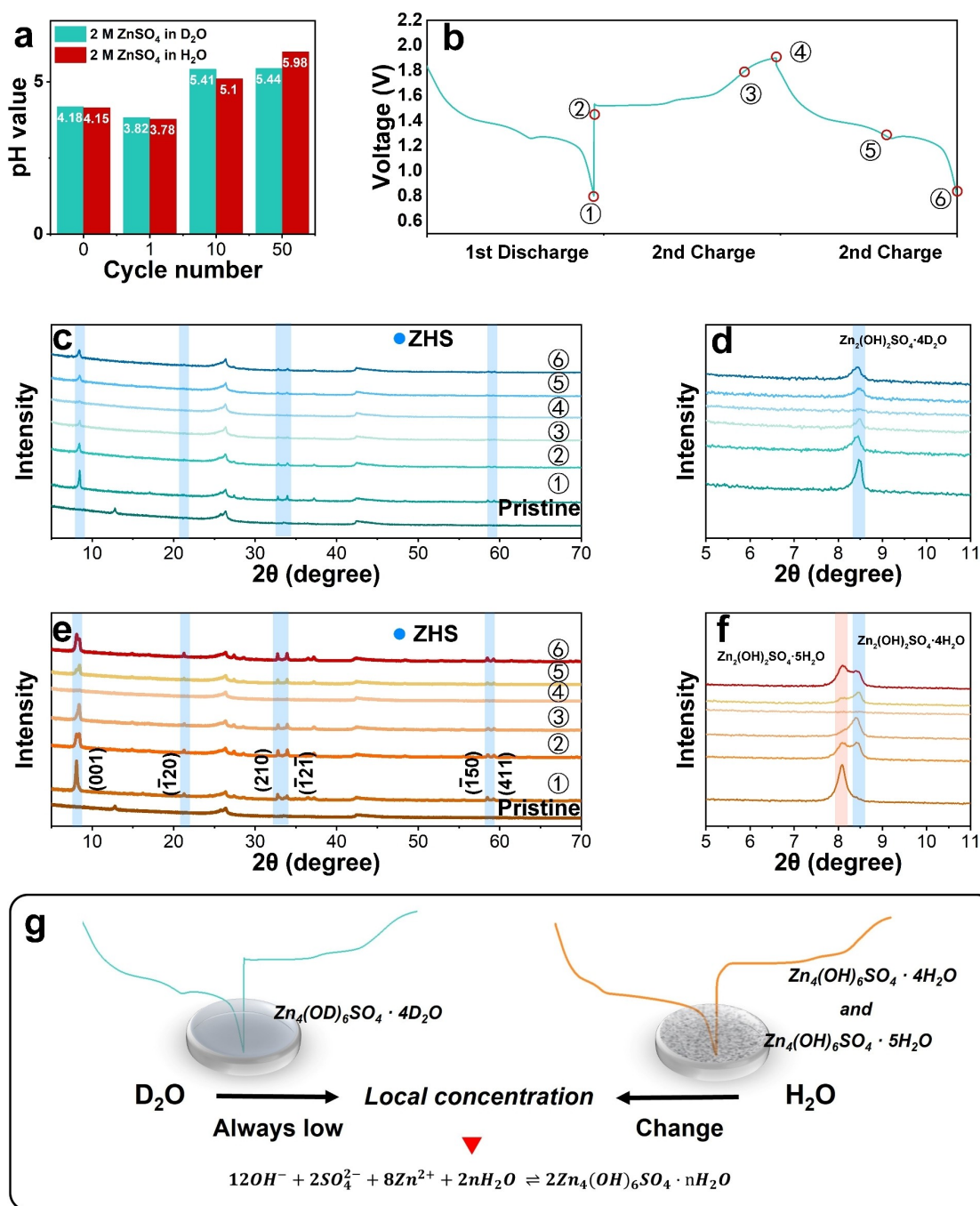
**Figure 4.** (a) In situ pH value recording of $D_2O$- and $H_2O$-based electrolytes. (b) Different states of Ex situ XRD spectra for the $MnO_2$ cathode after cycling at a current density of $2\,A\,g^{-1}$ in the full cell with (c) $D_2O$-based and (e) $H_2O$-based electrolyte. The amplified plots for the highest peak (001) in (d) $D_2O$-based and (f) $H_2O$-based electrolyte. (g) Schematic diagram of the effect of $D_2O$-based and $H_2O$-based electrolytes on the formation of ZHS on the cathode surface based on the differences in local concentration.

cules. When the concentration of water molecules at the electrode-electrolyte interface is sufficient, $Zn_2(OH)_2SO_4 \cdot 5H_2O$ tends to be generated. In the first discharge of the full cell in the $H_2O$-based electrolyte, $Zn_2(OH)_2SO_4 \cdot 5H_2O$ dominates and it is difficult to detect $Zn_2(OH)_2SO_4 \cdot 4H_2O$. With the progress of the cycle and the consumption of the electrolyte, the local concentration of water molecules is distributed nonuniformly at the interface between the electrode and the electrolyte, so that the mixed phase of $Zn_2(OH)_2SO_4 \cdot 4H_2O$ and $Zn_2(OH)_2SO_4 \cdot 5H_2O$ is produced at the second discharge. However, due to the strong coordination and low diffusion brought by $D_2O$, the $D_2O$-based electrolyte can keep the local concentration at a low level during the charging and discharging processes. Therefore, it is difficult to find $Zn_2(OH)_2SO_4 \cdot 5H_2O$ on the cathode for all

$D_2O$-based full cells. We believe that this suppression of the generation of different phases of the ZHS during cycling is beneficial and can provide a more stable interface between the electrolyte and electrodes.

To investigate the effect of EEI on the deposition and intercalation of $Zn^{2+}$ on the cathode in full cells, LSV tests from 0.8–1.9 V were performed in $D_2O$-based and $H_2O$-based electrolytes. As shown in Figure 5a, in the low potential region, the $H_2O$-based electrolyte performs HER more positive than the $D_2O$-based electrolyte, and the potential interval difference is ~0.26 V. In the high potential region, the oxidation peak potentials in $D_2O$-based and $H_2O$-based electrolytes are similar, with a difference of only 0.002 V. The effect of EEI on the electrochemical performance of $Zn\|MnO_2$ full cells were further investigated. As shown in Figure 5b, $D_2O$-based electrolytes were applied in $Zn\|MnO_2$ full cells for CV tests with a scan rate of 0.3 mV s$^{-1}$ in different potential windows of 0.8 to 1.9/2.0/2.1 V. During the charging process, two pairs of reduction and oxidation peaks were observed, the reduction peaks at 1.35 and 1.22 V, and the oxidation peaks at 1.56 and 1.61 V. The oxidation peak at 1.56 V gradually disappeared. The coin cell with $D_2O$-based electrolyte exhibited similar redox peak positions as the $H_2O$-based electrolyte (as shown in Figure S5), indicating the similarity of the two charge storage behaviors, which shows that during cycling in aqueous $ZnSO_4$ electrolyte, typical $MnO_2$-based cathodic redox reactions occur.[30] When the EW is extended to 0.8–2.0 and 2.1 V, the OER peak intensity of $D_2O$-based electrolyte does not show a large increase, which is quite different from the extremely strong OER generation in $H_2O$-based electrolyte under a wider potential window in Figure S5. In addition, during the cycling process of the $H_2O$-based electrolyte, the strong OER led to the change of the electrode structure, corresponding to a 0.02 V shift in the discharge peak position of the CV curve. In the $D_2O$-based electrolyte, the coincidence of the reduction peaks is still very high even after widening the EW. Cyclic voltammogram (CV) curves of the $D_2O$-based (as shown
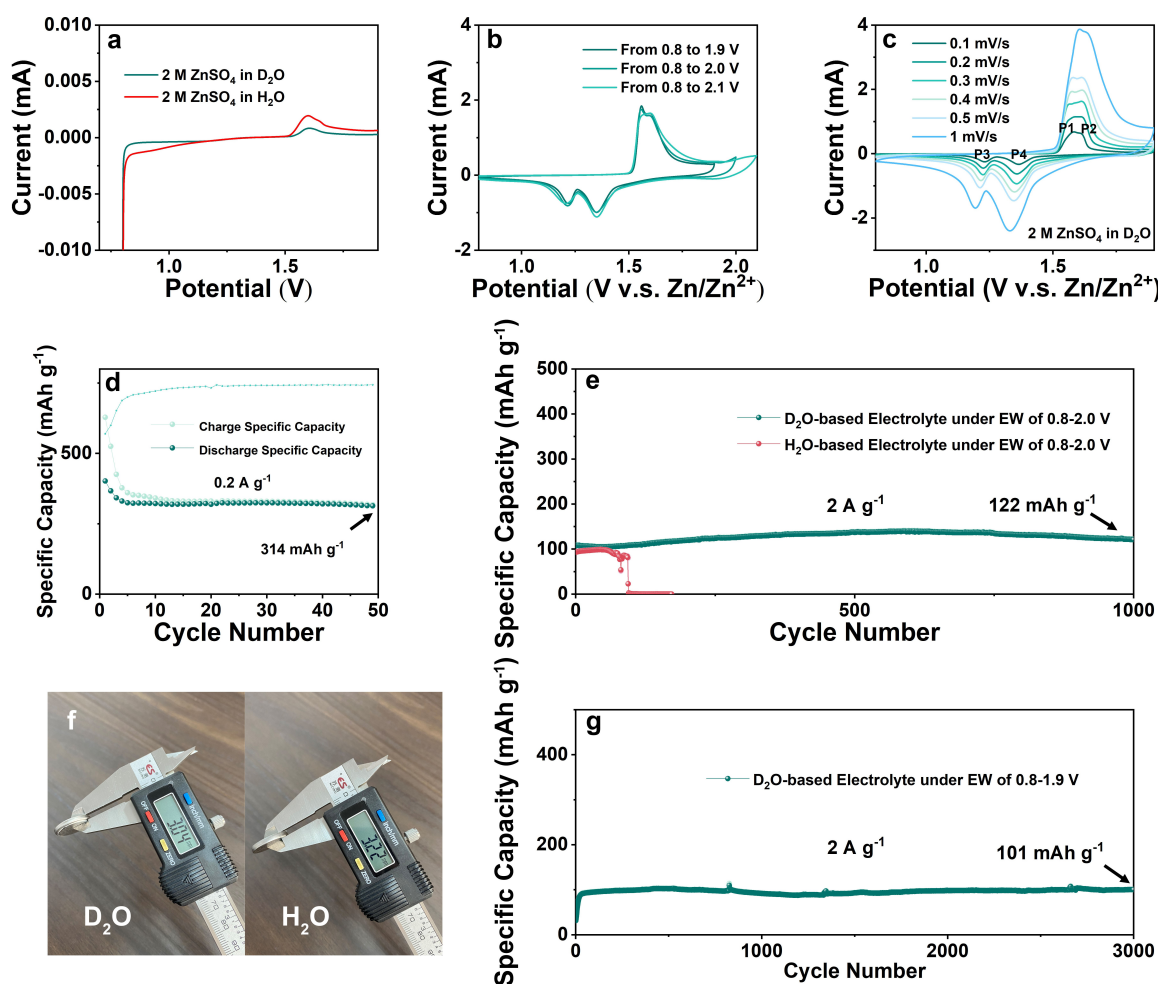


*Figure 5.* (a) LSV test of full cells of $D_2O$- and $H_2O$-based electrolytes in the range of 0.8–1.9 V. (b) CV test of $D_2O$-based electrolyte at a scan rate of 0.3 mV s$^{-1}$. (c) CV curves of $D_2O$-based electrolyte in the EW of 0.8–1.9 V with different scan rates. (d) Cycling performance of $D_2O$-based electrolytes in the EW of 0.8–2.0 V at a current density of 0.2 A g$^{-1}$. (e) Long-term cycling performance of $D_2O$-based electrolytes in the EW of 0.8–2.0 V at a current density of 2 A g$^{-1}$. (f) The thickness comparison of full cells with $D_2O$- and $H_2O$-based electrolytes after cycles in the EW of 0.8–2.0 V. (g) Long-term cycling performance of the full cells with $D_2O$-based electrolyte in the EW of 0.8–1.9 V at a current density of 2 A g$^{-1}$.

in Figure 5c) and $H_2O$-based electrolytes (as shown in Figure S6) in the normal EW of 0.8–1.9 V were measured at different scan rates of 0.1, 0.2, 0.3, 0.4, 0.5 and 1 mV s$^{-1}$, respectively, to discuss the effect of $D_2O$ on the electrochemical behavior of the Zn||MnO$_2$ full cells. For both $D_2O$-based and $H_2O$-based electrolyte, when the scan rate is low, two pairs of reduction and oxidation peaks were observed, with reduction peaks at 1.36 and 1.22 V and oxidation peaks at 1.56 and 1.61 V. As shown in Figure S6, the two pairs of redox peaks of the $H_2O$-based electrolyte start to overlap into a single pair from the scan rate of 0.3 mV s$^{-1}$. As the scan rate increases, the shifts of P2 and P4 are 0.054 and 0.045 V, respectively. In Figure 5c, ZIBs with $D_2O$-based electrolyte exhibit very similar CV curves at different scan rates, which shows that their charge/discharge mechanisms are similar at high and low rates. In contrast, the shifts of P1, P2, P3, and P4 in Figure 5c are only 0.022, 0.024, 0.031, and 0.027 V, respectively, which shows a more reversible electrochemical system formed by $D_2O$-based electrolyte.

The electrochemical performance in wide EWs requires cycling validation. The electrochemical profiles of cells with an EW of 0.8–2.0 V assembled with $D_2O$-based electrolyte at a current density of 0.2 A g$^{-1}$ are shown in Figure S7. During the charging and discharging process, the initial voltage platforms are located at about 1.55 and 1.30 V, which are consistent with the results of the CV test. As the cycle progresses, the charge and discharge platforms of the full cell assembled with $D_2O$-based electrolytes do not change significantly, indicating an extremely stable cycling performance. In the first cycle, most of the capacity in the charging process comes from the electron transferred by OER, which is caused by expanding the voltage window.[31] The $H_2O$-based electrolyte cannot complete this charging process, and all $H_2O$-based full cells are constantly performing OER during the charging process. Due to the slow diffusion of ions in $D_2O$, the OER is alleviated after the ion concentration on the electrode surface is reduced, allowing the full cells to continue to circulate. As shown in Figure 5d, the $D_2O$-based electrolyte exhibits stable cycling performance at EW of 0.8–2.0 V. Under the EW condition of 0.8–2.0 V, the $D_2O$-based electrolyte enables the full cells to reach a reversible capacity of 314 mAh g$^{-1}$ after 50 cycles. The electrochemical profiles of full cells with an EW of 0.8–2.0 V assembled with $D_2O$-based electrolyte at a current density of 2 A g$^{-1}$ are shown in Figure S6. Even if the EW is extended to 0.8–2.0 V, it still maintains a similar electrochemical behavior at the 1,000$^{th}$ cycle, demonstrating the remarkably wide EW cycling stability of the $D_2O$-based electrolyte. As shown in Figure 5e, the full cell with $H_2O$-based electrolyte collapsed after 73 cycles at EW of 0.8–2.0 V due to the strong side reactions. The massive gas accumulation during the cycling process increases the internal pressure, and the electrodes are forced to be separated, resulting in an open circuit. In stark contrast, the full cell with $D_2O$-based electrolyte can be stably cycled for more than 1,000 cycles at EW of 0.8–2.0 V and exhibit a reversible specific capacity of 122 mAh g$^{-1}$ at a

current density of 2 A g$^{-1}$ after 1,000 cycles. This is due to the $D_2O$-based electrolyte effectively suppressing OER and HER, as well as other aforementioned side reactions, even when the voltage is as high as 2.0 V.[32] the $H_2O$-based electrolyte, with high OER and HER activity, generates a large amount of gas, causing the cathode and anode of the full cells to quickly become open circuit. The difference can be easily observed even from the appearance of the battery, as shown in Figure 5f. The $D_2O$-based electrolyte can alleviate well the gas generation problem, and the full cell still maintains close to its initial thickness after 1,000 cycles at an EW of 0.8–2.0 V. The gas generation problem of $H_2O$-based electrolyte is very serious, and it is more obvious at a wider EW. The severe outgassing caused the expansion of the coin cell casing, and its thickness changed by about 50%, which seriously affected the stability and safety of the ZIBs. However, the low diffusion coefficient caused by EEI leads to an increase in the internal resistance of the ZIBs, as shown in Figure S7 for the EIS test of $D_2O$-based and $H_2O$-based electrolytes. In the ultra-high frequency region (> 10 kHz), in comparison to the ohmic resistance reflecting the transport of electrons and ions in the electrolyte, the $D_2O$-based electrolyte has a higher resistance ($R_s = 1.41\ \Omega$, $R_{ct} = 190.34\ \Omega$, $R_L = 58.32\ \Omega$) than the $H_2O$-based electrolyte ($R_s = 1.07\ \Omega$, $R_{ct} = 140.33\ \Omega$, $R_L = 56.637\ \Omega$), which indicates that the low-rate diffusion behavior of ions in $D_2O$. In the high frequency region, the resistance of the $D_2O$-based electrolyte is still higher than that of the $H_2O$-based electrolyte, indicating that the diffusion rate of $Zn^{2+}$ at the interface between the electrode and the $D_2O$-based electrolyte is lower than that of the $H_2O$-based electrolyte. In the low frequency region, the straight line corresponding to the solid-phase diffusion exhibits almost similar slopes, indicating that the EEI has no effect on the solid-phase diffusion of ions inside the electrode. When we examine the $D_2O$-based electrolyte with the commonly used EW of 0.8–1.9 V, it exhibits an excellent cycling performance. The reversible capacity of 101 mAh g$^{-1}$ can still be maintained after 3,000 cycles at a current density of 2 A g$^{-1}$, and its capacity retention rate is close to 100%. The ZIBs with $H_2O$-based electrolyte showed severe capacity decay and only displayed a specific capacity of 58 mAh g$^{-1}$, as shown in Figure S10. When the mixture of $D_2O$ and $H_2O$ is used as the solvent for the electrolyte, $D_2O$ can still significantly improve the stability of the ZIBs. As shown in Figure S11, when the volume ratio of $D_2O$ to $H_2O$ is 2:8, the Zn||MnO$_2$ full cell can exhibit a reversible capacity of 100 mAh g$^{-1}$ after 1000 cycles at a current density of 2 A g$^{-1}$. When the proportion of $D_2O$ was adjusted to 50% and 80%, the Zn||MnO$_2$ full cells could exhibit specific capacities of 105 and 109 mAh g$^{-1}$, as shown in Figures S12 and S13, after 1000 cycles at a current density of 2 A g$^{-1}$. The EEI brought by $D_2O$ applied to aqueous ZIBs can suppress OER, HER and other side reactions during cycling, which makes the $D_2O$-based electrolyte greatly promote the cycling stability of ZIBs.

## Conclusion

In conclusion, we reveal the application of the electro-chemical isotopic effect between heavy water ($D_2O$) and normal water ($H_2O$) electrolytes in ZIBs. Theoretical calculations show that compared with $H_2O$, the ion diffusion coefficient in $D_2O$ is lower, which can effectively suppress the generation of side reactions kinetics. Due to the kinetic and thermodynamic differences, $D_2O$-based aqueous electrolytes exhibit a wider electrochemical window than $H_2O$-based electrolytes, showing limited electroactivity for OER/HER, less pH value change, and generation of ZHS. Through the change of bound water in ZHS during cycling, it was found for the first time that $D_2O$ suppresses the generation of different ZHS phases during cycling, thus providing a more stable electrode-electrolyte interface. By using $D_2O$-based electrolyte, aqueous ZIBs with $MnO_2$ cathode and metallic Zn anode exhibited a specific capacity of $122\ \mathrm{mAh\,g^{-1}}$ after 1000 cycles at a current density of $2\ \mathrm{A\,g^{-1}}$ at EW of 0.8–2.0 V, demonstrating an excellent cycle life. Due to the miscibility of $D_2O$ and $H_2O$, and the price of $D_2O$ ($< 1.5$ USD/ g) is comparable to traditional electrolyte solvents/ additives of ZIBs, our strategy can provide insights into the rational design and flexible production of electrolytes for aqueous batteries. Moreover, the change of ZHS in the cycling process will also be a direction worth pursuing. More importantly, our study shows that improving the reaction kinetics is an effective way to improve the stability and long-term cycling performance of ZIBs.

## Acknowledgements

## Conflict of Interest

The authors declare no conflict of interest.

## Data Availability Statement

The data that support the findings of this study are available from the corresponding author upon reasonable request.

[1] a) Y. Dai, X. Liao, R. Yu, J. Li, J. Li, S. Tan, P. He, Q. An, Q. Wei, L. Chen, *Adv. Mater.* **2021**, *33*, 2100359; b) X. Gao, C. Zhang, Y. Dai, S. Zhao, X. Hu, F. Zhao, W. Zhang, R. Chen, W. Zong, Z. Du, *Small Structures* **2022**, 2200316.

[2] a) D. J. Adams, P. J. Dyson, S. J. Tavener, *Chemistry in alternative reaction media*, John Wiley & Sons, **2005**; b) Q. Li, Y. Wang, F. Mo, D. Wang, G. Liang, Y. Zhao, Q. Yang, Z. Huang, C. Zhi, *Adv. Energy Mater.* **2021**, *11*, 2003931.

[3] J. Chou, Y. Zhao, X. T. Li, W. P. Wang, S. J. Tan, Y. H. Wang, J. Zhang, Y. X. Yin, F. Wang, S. Xin, *Angew. Chem., Int. Ed.* **2022**, e202203137.

[4] R. Chen, H. Tang, Y. Dai, W. Zong, W. Zhang, G. He, X. Wang, *ACS Nano* **2022**, *16*, 19124.

[5] a) L. Ma, C. Zhi, *Electrochem. Commun.* **2021**, *122*, 106898; b) Y. Geng, L. Pan, Z. Peng, Z. Sun, H. Lin, C. Mao, L. Wang, L. Dai, H. Liu, K. Pan, *Energy Storage Mater.* **2022**, *51*, 733.

[6] a) W. Zhang, Y. Wu, Z. Xu, H. Li, M. Xu, J. Li, Y. Dai, W. Zong, R. Chen, L. He, *Adv. Energy Mater.* **2022**, 2201065; b) W. Zong, H. Guo, Y. Ouyang, L. Mo, C. Zhou, G. Chao, J. Hofkens, Y. Xu, W. Wang, Y. E. Miao, *Adv. Funct. Mater.* **2022**, *32*, 2110016; c) J. Zhu, L. Xia, W. Yang, R. Yu, W. Zhang, W. Luo, Y. Dai, W. Wei, L. Zhou, Y. Zhao, *Energy Environ. Sci.* **2022**, *5*, 655; d) X. Gao, X. Sun, J. Liu, N. Gao, H. Li, *J. Energy Storage* **2019**, *25*, 100901.

[7] W. Zhang, Y. Dai, R. Chen, Z. Xu, J. Li, W. Zong, H. Li, Z. Li, Z. Zhang, J. Zhu, *Angew. Chem., Int. Ed.* **2022**, *62*, e202212695.

[8] F. Soddy, *Sci Mon.* **1923**, *17*, 305.

[9] L. Curtiss, D. Frurip, M. Blander, *J. Chem. Phys.* **1979**, *71*, 2703.

[10] a) X. Gao, X.-Y. Yu, C.-R. Chang, *Phys. Chem. Chem. Phys.* **2022**, *24*, 15182; b) M. H. Thiemens, M. Lin, *Rev. Mineral. Geochem.* **2021**, *86*, 35.

[11] J. Van Rooyen, Stellenbosch: Stellenbosch University, **2021**.

[12] S. Cai, T. Bai, H. Chen, W. Fang, Z. Xu, H. Lai, T. Huang, H. Xu, X. Chu, J. Ling, *J. Phys. Chem. Lett.* **2019**, *11*, 303.

[13] K. Kopple, D. Meyerstein, D. Meisel, *J. Phys. Chem.* **1980**, *84*, 870.

[14] J. Saha, J. Podder, *J. Bangladesh Acad. Sci.* **2011**, *35*, 203.

[15] W. Cui, Y. Zheng, R. Zhu, Q. Mu, X. Wang, Z. Wang, S. Liu, M. Li, R. Ran, *Adv. Funct. Mater.* **2022**, *32*, 2204823.

[16] S. Ghosh, S. Ullah, J. P. de Mendonça, L. G. Moura, M. G. Menezes, L. S. Flôres, T. S. Pacheco, L. F. de Oliveira, F. Sato, S. O. Ferreira, *Spectrochim. Acta A Mol. Biomol. Spectrosc.* **2019**, *218*, 281.

[17] J. H. Lee, B. M. Tackett, Z. Xie, S. Hwang, J. G. Chen, *Chem. Comm.* **2020**, *56*, 106.

[18] M. Nielsen, M. E. Björketun, M. H. Hansen, J. Rossmeisl, *Surf. Sci.* **2015**, *631*, 2.

[19] a) Z. Xu, Q. Fan, Y. Li, J. Wang, P. D. Lund, *Renewable Sustainable Energy Rev.* **2020**, *127*, 109838; b) J. Cao, D. Zhang, C. Gu, X. Zhang, M. Okhawilai, S. Wang, J. Han, J. Qin, Y. Huang, *Nano Energy* **2021**, *89*, 106322.

[20] Y. Tang, C. Liu, H. Zhu, X. Xie, J. Gao, C. Deng, M. Han, S. Liang, J. Zhou, *Energy Storage Mater.* **2020**, *27*, 109.

[21] R. Li, M. Li, Y. Chao, J. Guo, G. Xu, B. Li, Z. Liu, C. Yang, *Energy Storage Mater.* **2022**, *46*, 605.

[22] Y. Zhang, P. Srimuk, S. Husmann, M. Chen, G. Feng, V. Presser, *J. Electrochem. Soc.* **2019**, *166*, A4158.

[23] a) Y. Lv, Y. Xiao, L. Ma, C. Zhi, S. Chen, *Adv. Mater.* **2022**, *34*, 2106409; b) K. Zhou, N. Wang, X. Qiu, H. Xie, P. Wei, X. Dong, Y. Wang, *ChemSusChem* **2022**, *15*, e202201739; c) Z. Yang, C. Lv, W. Li, T. Wu, Q. Zhang, Y. Tang, M. Shao, H. Wang, *Small* **2022**, *18*, 2104148.

[24] a) A. Otsuki, L. De Campo, C. J. Garvey, C. Rehm, *Colloids Interfaces* **2018**, *2*, 37; b) X. Zhou, L. Wang, X. Fan, B. Wilfong, S.-C. Liou, Y. Wang, H. Zheng, Z. Feng, C. Wang, E. E. Rodriguez, *Chem. Mater.* **2020**, *32*, 769.

[25] S. Chen, P. Sun, J. Humphreys, P. Zou, M. Zhang, G. Jeerh, S. Tao, *Energy Storage Mater.* **2021**, *42*, 240.

[26] P. J. McHugh, A. D. Stergiou, M. D. Symes, *Adv. Energy Mater.* **2020**, *10*, 2002453.

[27] a) C. Huang, Q. Wang, D. Zhang, G. Shen, *Nano Res.* **2022**, *15*, 8118; b) A. Bayaguud, X. Luo, Y. Fu, C. Zhu, *ACS Energy Lett.* **2020**, *5*, 3012.

[28] P. Yadav, N. Kumari, A. K. Rai, *J. Power Sources* **2023**, *555*, 232385.

[29] a) T. Xue, H. J. Fan, *J. Energy Chem.* **2021**, *54*, 194; b) K. Zhu, T. Wu, S. Sun, Y. Wen, K. Huang, *ChemElectroChem* **2020**, *7*, 2714.

[30] I. A. Rodríguez-Pérez, H. J. Chang, M. Fayette, B. M. Sivakumar, D. Choi, X. Li, D. Reed, *J. Mater. Chem. A* **2021**, *9*, 20766.

[31] a) J. Hu, A. Al-Salihy, J. Wang, X. Li, Y. Fu, Z. Li, X. Han, B. Song, P. Xu, *Adv. Sci.* **2021**, *8*, 2103314; b) J. Zhu, L. Xia, R. Yu, R. Lu, J. Li, R. He, Y. Wu, W. Zhang, X. Hong, W. Chen, *J. Am. Chem. Soc.* **2022**, *144*, 15529.

[32] Y. Du, Y. Li, B. B. Xu, T. X. Liu, X. Liu, F. Ma, X. Gu, C. Lai, *Small* **2022**, *18*, 2104640.

# Research Articles

**Zn-Ion Batteries**

X. Gao, Y. Dai, C. Zhang, Y. Zhang,
W. Zong, W. Zhang, R. Chen, J. Zhu, X. Hu,
M. Wang, R. Chen, Z. Du, F. Guo, H. Dong,
Y. Liu, H. He, S. Zhao, F. Zhao, J. Li,
I. P. Parkin, C. J. Carmalt,
G. He* —————————— e202300608

When It's Heavier: Interfacial and Solvation Chemistry of Isotopes in Aqueous Electrolytes for Zn-ion Batteries



Cathode

Low local concentration
→
Pure phase ZHS precipitation

More stable pH

Slow & uniform deposition

Metallic Zn    ● $Zn^{2+}$    ☩ $SO_4^{2-}$

$D_2O$-based electrolyte

The electrochemical effect of isotope of water is introduced into a Zn-ion battery electrolyte to control severe side reactions and massive gas production. Due to the low diffusion and strong coordination of ions in $D_2O$, the possibility of side reaction is decreased, resulting in a broader electrochemically stable potential window, less pH change, less zinc hydroxide sulfate (ZHS) generation and pure phase ZHS precipitation during cycling.